Int. J. Heat Mass Transfer. Vol. 5, pp. 595–614. Pergamon Press 1962. Printed in Great Britain.

ECCENTRIC ROD BURNOUT AT 1000 lbf/in² WITH NET STEAM GENERATION

S. LEVY, E. E. POLOMIK, C. L. SWAN and A. W. McKINNEY
Atomic Power Equipment Department, General Electric Company, San Jose, California

(*Received* 18 *August* 1961 *and in revised form* 17 *January* 1962)

Abstract—Burnout and pressure-drop tests were performed with an eccentric rod geometry to simulate possible maldistribution of flow in multirod fuel assemblies of boiling-water reactors. Data are presented for a uniformly heated rod, 0·540 in in dia. and 8½ ft long, located within a circular pipe of 0·875 in i.d. Test variables include one concentric and three displaced rod geometries, exit steam qualities from 9 to 66 per cent by weight, flow rates from 0·25 to $1{\cdot}34 \times 10^6$ lb/h ft² and system pressures of 1000 lbf/in². Test results are as follows:

(1) Burnout heat fluxes with net steam generation are the same for the concentric annulus of 0·1675 in and the eccentric flow spacing of 0·096 and 0·061 in. Burnout values decrease by 15–36 per cent when the minimum flow annulus is reduced from 0·1675 to 0·033 in.

(2) Single-phase pressure-drop tests exhibit a decrease in friction factor as the eccentricity increases. On the other hand, two-phase pressure losses remain relatively the same at various eccentricities.

(3) An analytical model is postulated to determine the degree of transverse mixing in an eccentric geometry. The model based upon subdividing the flow area into two parallel channels indicates that mixing extends well over half of the flow zone.

INTRODUCTION

STEAM distribution is seldom uniform at every cross section of a multirod fuel assembly (see Fig. 1). Uneven power generation and different flow characteristics often produce local variations in steam quality. In particular, the corner rod sometimes exhibits the highest heat production combined with the lowest hydraulic diameter. These conditions could lead to higher steam qualities or "channeling" at the corner, and the burnout heat flux there could not be specified without previous establishment of the degree of "channeling" produced by the proximity of the corner rod to the fuel assembly channel.

Conditions at the corner rod can be *approximately simulated* by use of an eccentric rod within a circular pipe. Because the ability of the fluid to flow around the eccentric rod is much less in the case of a corner rod in a fuel bundle as compared to an eccentric rod in a circular pipe, tests with a circular pipe tend to overestimate the effects of fuel-rod eccentricities. Still, various eccentricity settings can be utilized in a circular pipe to reproduce spacings of corner rod to channel and possible variations with manufacturing tolerances. Burnout tests have been performed with such a simplified geometry and are described in this report.

Burnout results with net steam generation in eccentric annuli are not available in the literature. However, pressure-drop and heat-transfer results in an eccentric vertical annulus at pressures close to atmospheric are given in [1]. Also, burnout measurements at 1000 lbf/in² for concentric annuli are reported in [2] for horizontal flow and in [3] for vertical flow. Finally, a complete summary of burnout studies for water with net steam generation is given in [4]. The data covered therein include test results in rectangular channels and round tubes at pressures between 500 and 3000 lbf/in².

DESCRIPTION OF EQUIPMENT

Test loop

The test facility as depicted in Fig. 2 is comprised of two stainless-steel loops into which are inserted flanged pipe sections containing the electrically heated test sections. Steam generated in either loop passes to an air-cooled condenser

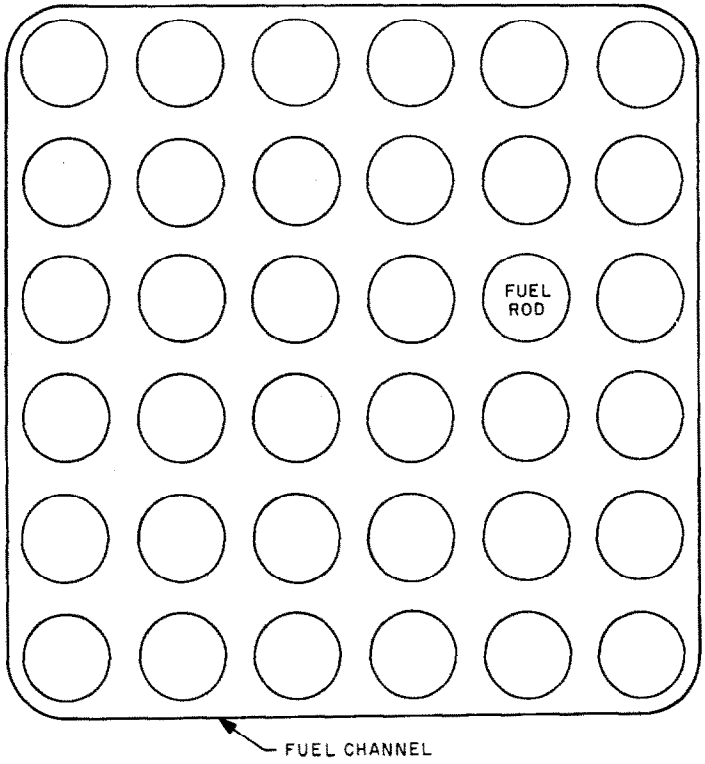

FIG. 1. Multirod fuel assembly.

where it is converted to saturated liquid before being returned to the main circuit. Subcooling is achieved by removal of saturated liquid from the loop, from where it is passed through another air cooler and then returned to the loop upstream of the test section. A suitable transformer with an induction regulator for voltage control provides a.c. electrical power to the test elements. A control panel placed adjacent to the loops contains the necessary indicating and recording instruments and controls. A detailed description of the facility is given in [5].

Test section

The test section is shown in Fig. 3. Water enters at the bottom of the test section and flows upwards in the annulus between an electrically heated tube of 0·540 in o.d. and a stainless-steel pipe of 0·875 in i.d. The heater tube, made of 304 stainless-steel, is 8 ft 6 in long and has a 0·049-in wall thickness. It is positioned within the outer pipe by means of groups of three spacers shown in Fig. 3. The three spacers are located 1 in and 120° apart. Additional single spacers are provided to prevent electrical shorting and to maintain the close spacing required on the narrow annulus or eccentric side of the test section. Each spacer, as shown in Fig. 3, consists of a sapphire rod 0·220 in in dia. backed by a stainless-steel plug.

Positioning of the rod is obtained by initial contact being made between the rod and outer pipe on the eccentric side. Reference readings are then taken for all spacers from the extremity of the stainless-steel plug to the diametrically outer radius of the external pipe. The two spacers on the non-eccentric side are next withdrawn an amount about 10 mils in excess of that required for the rod setting. The eccentric spacers are inserted the required distance and tightened into position. The non-eccentric spacers are finally tightened. The position of the rod could be, and was, verified by measurements through the pressure tap holes. These measurements indicate

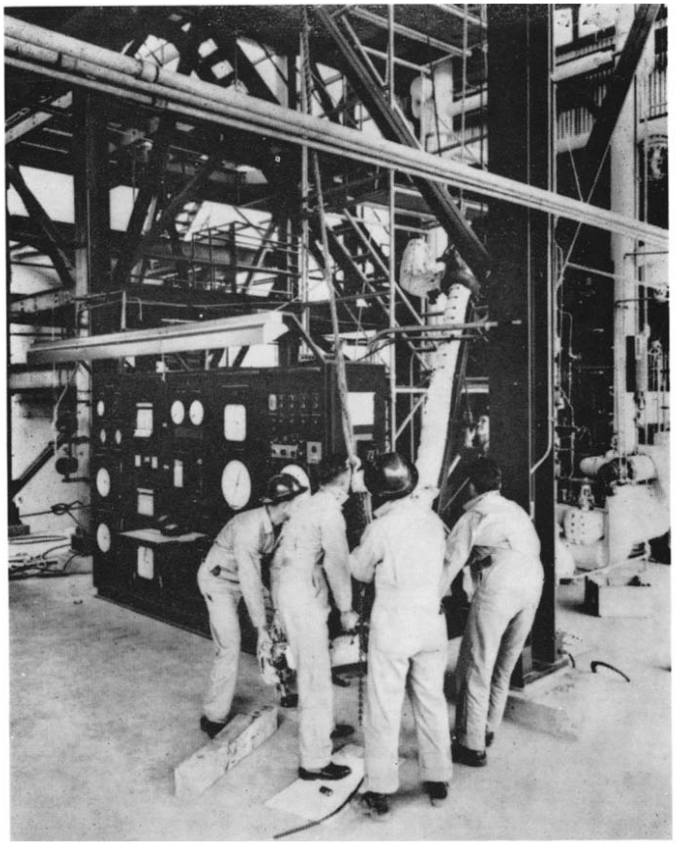

FIG. 2. Heat-transfer facility.

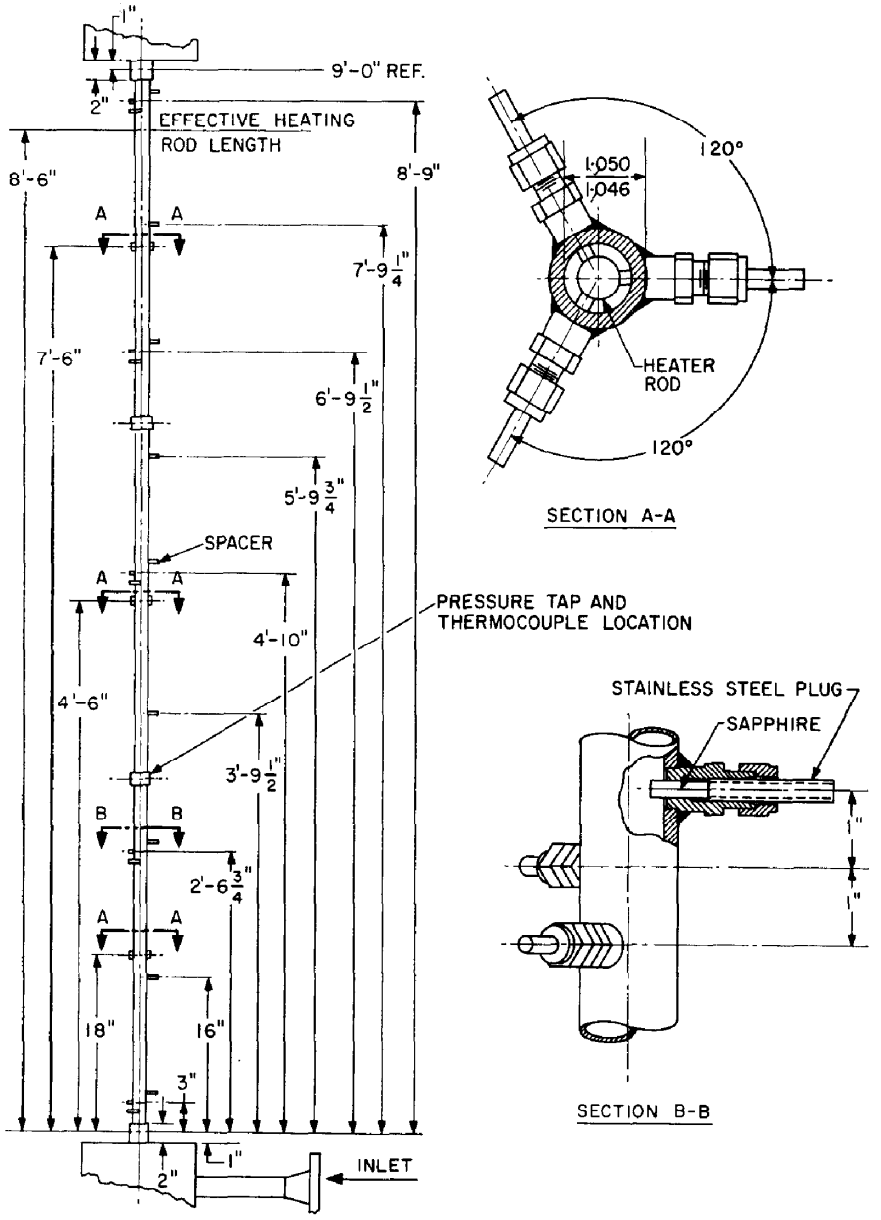

FIG. 3. Test section.

that the heater-rod location was known within ~6 mils.

Pressure drop and water temperatures are measured at various levels along the test section. Chromel–alumel thermocouples in a $\frac{3}{16}$-in dia. stainless-steel well are installed in the steam–water flow at the 0, $1\frac{1}{2}$, 3, $4\frac{1}{2}$, 6, $7\frac{1}{2}$ and 9 ft levels and barely extend in the flowing steam. Pressure taps are located at the same levels. Each pressure tap is connected to a seal pot, and the seal pot to a common pressure manifold.

Thermocouples are installed inside the heater rod. Thermocouples made of chromel–alumel wire are spot-welded inside the rod at various positions. Four thermocouples are located at the exit end of the rod while two more are installed 1 and 2 ft from that end. The thermocouple leads are brought out of the test section through the hollow-bottom electrical conductor.

Instrumentation and control

The loops are instrumented to indicate and record power supplied to the test section, pressure and flow. The instruments and readings are as follows:

(1) An Ashcraft 2000 lb gauge and two Heise gauges from 0–1100 and 800–1600 lb/in^2 to determine the loop pressure.
(2) Orifices and Foster flow tubes installed in the down-comer and cross-over to the pump respectively to measure the loop recirculation rate.
(3) A recording watt-meter, a watt-hour meter, and an indicating voltmeter and ammeter to obtain the power input to the test section.

EXPERIMENTAL ERRORS

Burnout measurements are effectively represented by the plot of heat flux versus steam quality. The accuracy of the test results can thus be evaluated by means of the errors associated with these two parameters.

Heat flux

Uniform heat generation was used in all of the present tests, and the heat flux at the burnout point can be computed by dividing the power input to the test section by its heat-transfer area. The main errors in such computed values result from the inaccuracy of the power readings and the assumption that the average rod heat flux is identical to the local one at the top of the heater rod.

For heat fluxes above 10^6 Btu/h ft^2 (~ 400 kW) the maximum error is estimated to be 5·7 per cent if 0·2 per cent error is allowed for tolerances in rod dimensions, i.e. heat-transfer area. The corresponding uncertainty interval for a 95 per cent confidence level in burnout heat flux can be obtained by the method of Kline and McClintock [6]. It is about 3 per cent at the highest flux value of the present tests.

Steam quality

The exit steam weight fraction or quality is obtained from a simple enthalpy balance

$$x = \frac{Q/w - (h_f - h_i)}{h_{fg}} \tag{1}$$

where

x = steam quality by weight,
Q = heat generated in rod, Btu/h,
w = flow rate, lb/h,
h_f = enthalpy of saturated water, Btu/lb,
h_i = enthalpy of water at inlet conditions, Btu/lb,
h_{fg} = heat of vaporization, Btu/lb.

The flow rate w is calculated from standard orifice equations.

Table 1. Uncertainty in exit steam quality

Pressure (lbf/in^2)	Mass flow (lb/s)	Subcooling (Btu/lb)	Power (kW)	Exit quality (wt.—%)	Quality error
1000	0·839	114·5	180	13·1	0·88
1000	0·796	35·4	122·4	16·5	1·60
1000	0·295	85·0	80	26·5	2·32
1000	0·353	69·9	100	30·7	2·03

The method of Kline and McClintock [6] has been applied to equation (1) to establish the uncertainty in steam quality. Typical uncertainty values in the exit steam quality values are given in Table 1. These numbers yield a 95 per cent confidence level.

The values in Table 1 reveal that the uncertainty interval approaches at most 10 per cent. The corresponding uncertainty interval in exit enthalpy is about 2·3–2·5 per cent.

BURNOUT DETECTION

Rod element burnout was detected by a Safety Monitor System which causes the main power circuit breaker to trip when burnout conditions are impending. The system relies upon an electronic circuit which monitors the balance between the voltages measured across two adjacent 1-ft sections at the exit end of the rod. This voltage remains in balance during normal operation, at which time a pair of thyratron tubes firing on alternate half-cycles hold a relay open in the breaker trip circuit.

Burnout produces a sudden increase in rod resistance. This leads to an unbalanced input voltage to the Safety Monitor circuit. The unbalance prevents one thyratron tube from firing which de-energizes the relay in the breaker circuit, causing trip. The sensitivity of the circuit to a voltage unbalance can be adjusted so that, in effect, the temperature at which trip occurs can be selected. The circuit time constant is less than 8 ms.

Very satisfactory and reliable operation of the trip system has been obtained to date. However, in order to verify that the Safety Monitor trip was caused by a temperature rise at the exit end of the uniform wall rod a 30-gauge thermocouple wire was attached internally to the rod at that point. This thermocouple temperature was recorded on a fast-response Sanborn instrument and temperature traces obtained at burnout conditions. A typical trace is shown in Fig. 4. The thermocouple reading remains practically constant as the input power to the heater rod is raised to approach burnout. Just before burnout,

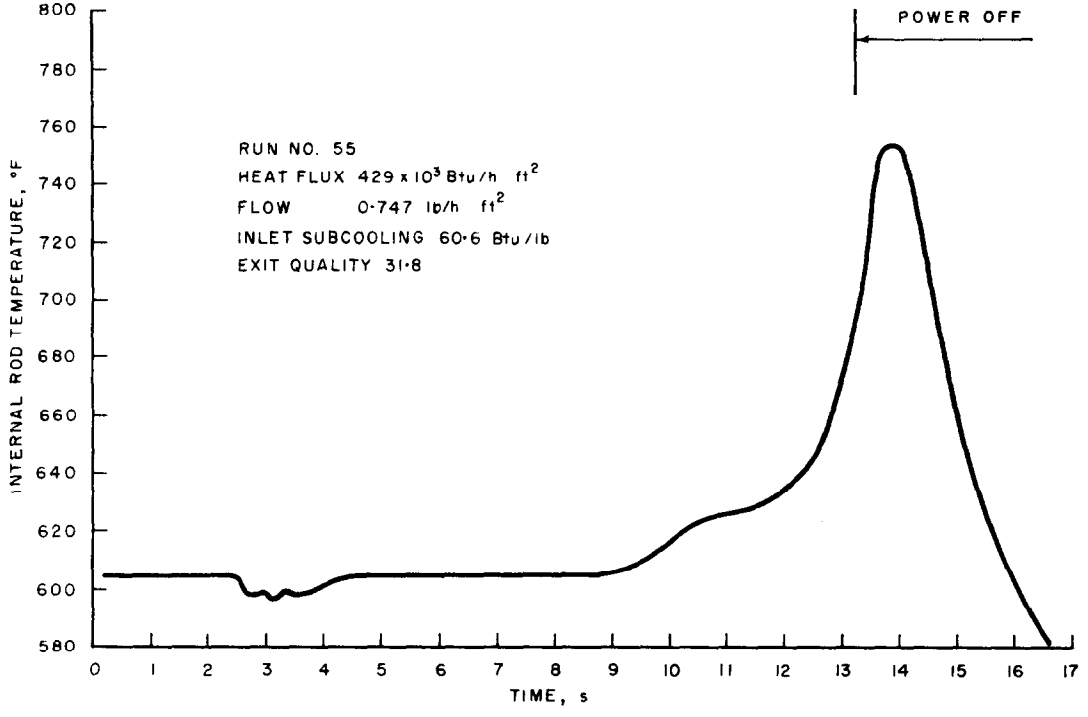

FIG. 4. Typical temperature trace at burnout.

a small change in power produces a very large increase in temperature. As shown in Fig. 4, the temperature rise stops only when the power is turned off. *A monitor trip and a trace of the type shown in Fig. 4 were simultaneously obtained for every burnout run.*

Continuous temperature recordings at the exit end of the heater rod offer several other advantages. They make it possible to determine the time and temperature range of a burnout point and to investigate the effects of heat flux and quality upon the mode of burnout. Before a large number of temperature traces are examined, it is worthwhile to note that burnout conditions can be approached by varying any one of three variables (power, subcooling or flow) while maintaining the other two constants. Immediate burnout response is obtained by increasing the power; the response is somewhat delayed for changes in subcooling or flow. In all three cases, however, it was found that burnout was a sharply defined point. A 2°F change in subcooling at fixed flow and power settings would produce a sudden temperature rise, as shown in Fig. 5(a). The temperature decreases if the subcooling is increased (about 1°F) and rises again to produce burnout when subcooling is lowered.

Four traces are shown in Fig. 5. The traces (a) and (b) represent fluctuating high "film boiling" temperatures before burnout. These are representative of low heat flux conditions. Fig. 5(c) and (d) show the sharp temperature rises obtained at high heat flux.

Data repeatability

The first burnout point taken for a given rod setting was repeated at the end of each operating day. This served to establish not only that burnout results were repeatable, but also to verify that the test-section geometry was relatively preserved. Typical data repeatability is illustrated in Table 2 for a minimum flow annulus of 0·096 in:

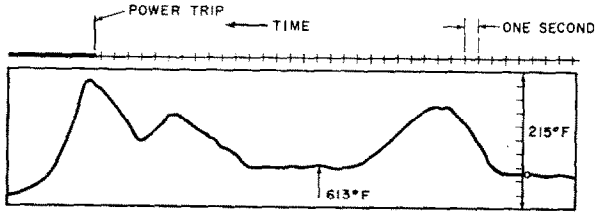

TRACE 5 (a) RUN NO. 59; HEAT FLUX 436 X 10^3 Btu/h. ft^2; EXIT QUALITY 30·4 PER CENT

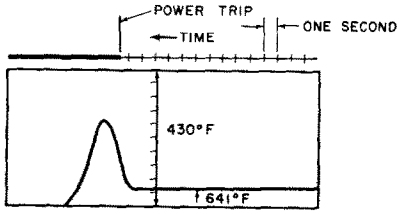

TRACE 5 (c) RUN NO. 63; HEAT FLUX 663·000 Btu/h ft^2; EXIT QUALITY 18·6 PER CENT

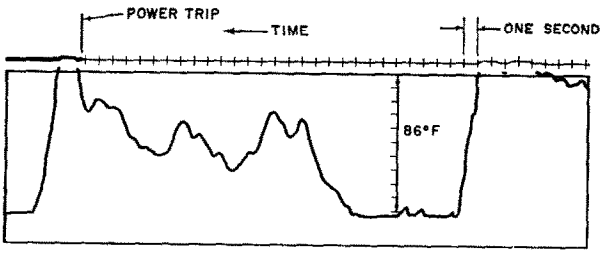

TRACE 5 (b) RUN NO. 56; HEAT FLUX 422 000 Btu/h ft^2; EXIT QUALITY 48·1 PER CENT

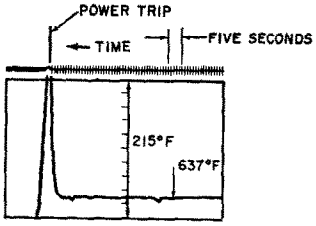

TRACE 5 (d) RUN NO. 42; HEAT FLUX 997·000 Btu/h ft^2; EXIT QUALITY 21 PER CENT

FIG. 5. Internal-rod temperature traces at burnout.

Table 2. Data repeatibility

Run	Flow (lb/h ft²)	Subcooling (Btu/lb)	Pressure (lbf/in²)	Heat flux (Btu/h ft²)	Exit quality (wt.—%)
49	$0{\cdot}772 \times 10^6$	58·8	955	448×10^3	32·1
53	$0{\cdot}765 \times 10^6$	60·0	998	439×10^3	31·8
55	$0{\cdot}747 \times 10^6$	60·0	1002	429×10^3	31·8
59	$0{\cdot}776 \times 10^6$	64·0	1006	436×10^3	30·4

Data reduction

Data reduction from day to day was utilized to determine test data deviations and the next run settings. Additional and repeat runs were initiated whenever required.

Hydraulic stability

Pressure drop across the test section was recorded as the burnout point was approached. Each power increase at constant subcooling and flow is accompanied by an increase in pressure drop. Examination of the traces determines the degree of hydraulic stability before burnout. Two typical traces are shown in Fig. 6. Fig. 6(a) corresponds to stable runs, while Fig. 6(b) shows the smallest degree of hydraulic stability achieved in the tests. Note that the pressure taps were all located on the eccentric rod side.

TEST RESULTS—PRESSURE DROP

Single-phase flow

Pressure drop was measured for *cold-water flow without heat addition.* A typical set of pressure-drop runs is plotted in Fig. 7 for an 0·096 in minimum flow annulus. It is noted that the frictional and spacer losses can be approximated by means of straight lines. This is understandable, since the spacers are about uniformly distributed between pressure taps, and fully developed flow is established beyond the 1½-ft position.

If the spacer losses are estimated by means of accepted contraction–expansion formulas* for each eccentric geometry, the experimental results can be applied to calculate friction factors.

* Spacer losses account for 7–22 per cent of the measured pressure-drop losses.

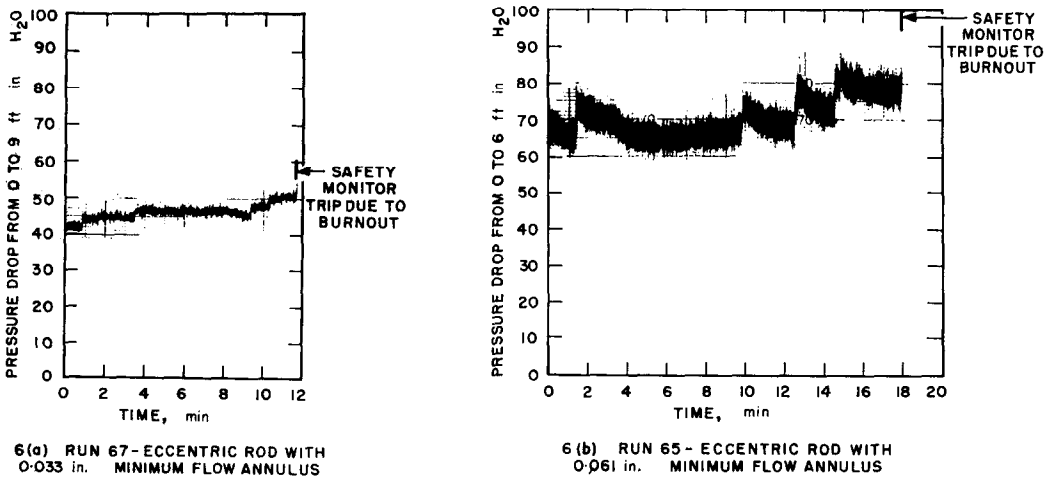

6(a) RUN 67 - ECCENTRIC ROD WITH 0·033 in. MINIMUM FLOW ANNULUS

6(b) RUN 65 - ECCENTRIC ROD WITH 0·061 in. MINIMUM FLOW ANNULUS

FIG. 6. Pressure-drop traces illustrating system hydraulic stability.

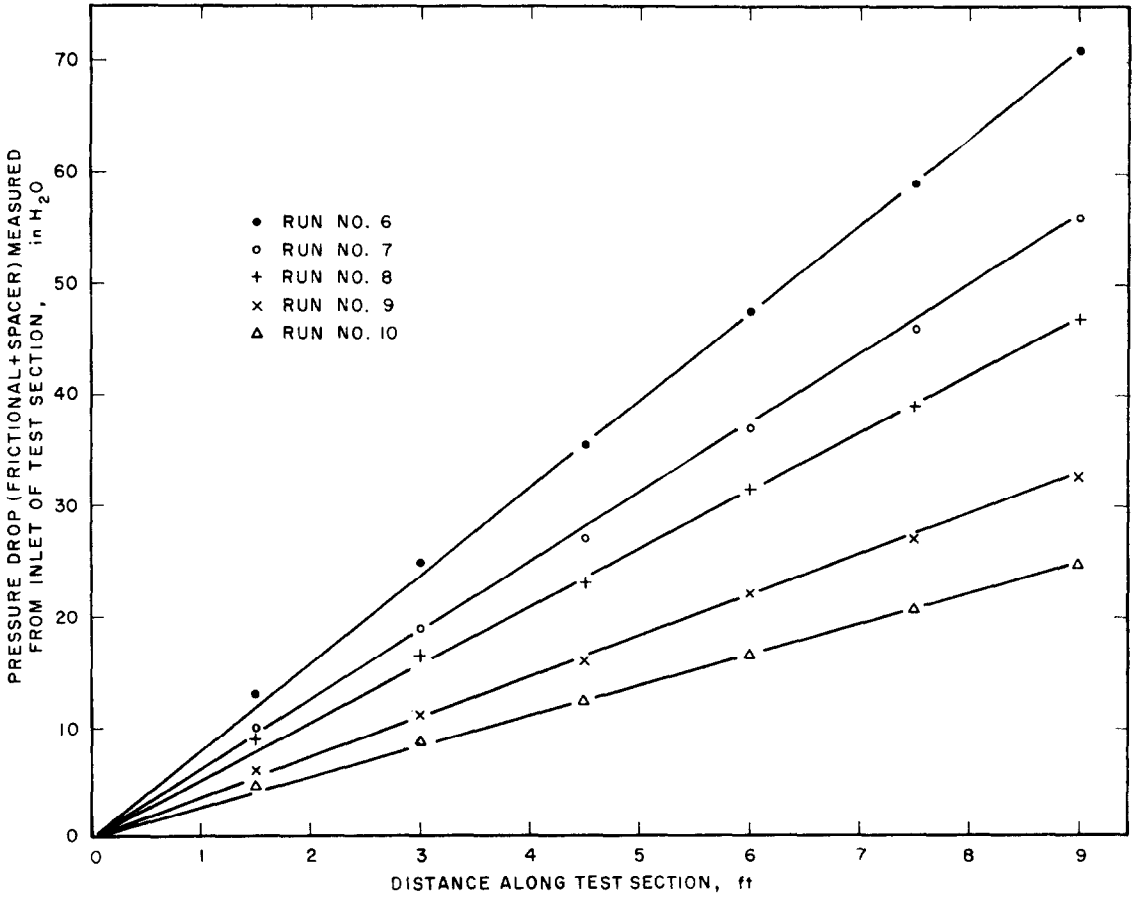

FIG. 7. Single-phase pressure-drop data for eccentric rod with 0·096 in minimum flow annulus.

It is possible to calculate a friction factor for each of the tap readings, as illustrated below for a typical run, Run no. 7 of Fig. 7.

position	0–1½ ft	0–3 ft	0–4½ ft
f, friction factor	0·0283	0·0271	0·0276
position	0–6 ft	0–7½ ft	0–9 ft
f, friction factor	0·0275	0·0276	0·0274

The accuracy of the computed friction factor is expected to improve with distance along the test section. This is due to the larger pressure-drop reading and the smaller effect of the ~1-in error in the transmitters. For this reason, only the readings from 0–9 ft were used in Fig. 8 to determine the effect of eccentricity upon friction factor. However, it is worthwhile to note the small deviation in friction factor with position for Run no. 7. It means that each of the 0–9 ft values plotted in Fig. 8 corresponds to about six points. Examination of Fig. 8 reveals that the friction factor decreases as the eccentricity increases. This result agrees with the test data of [1]. A 30 per cent decrease in friction factor was reported there for a $\frac{1}{8}$ in annulus of 1·08 in i.d. when the flow annulus was reduced by 30 per cent on one side. The present tests predict a smaller effect of eccentricity and are in agreement with more recent studies [7]. Tentative friction-factor lines have been drawn for each geometry in Fig. 8. In the drawing of mean friction factor lines special emphasis was placed upon the runs at high velocity (i.e. high pressure drop and high Reynolds number).

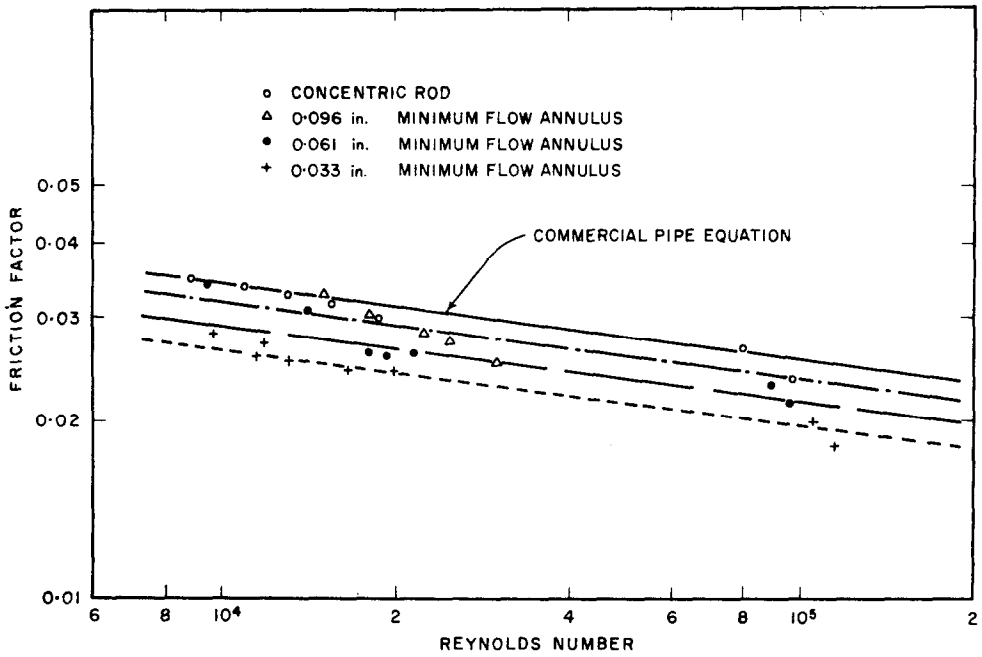

FIG. 8. Single-phase friction factor for eccentric rod.

Further, the concentric rod line was selected to agree with the friction-factor equation for commercial pipe, namely

$$f = 0{\cdot}160/N_{Re}^{0{\cdot}16}$$

where N_{Re} = Reynolds number, non-dimensional.

To verify that the previous trends were preserved at high temperature, heated runs with high subcooling and without local boiling were utilized to obtain points in the Reynolds number range of 10^5. Properties were evaluated at the bulk conditions between tap 0 and tap 1½ ft, and tap 1½ and 3 ft. The friction factor as plotted in Fig. 8 was corrected by the ratio $(\mu_b/\mu_w)^{0{\cdot}14}$ to account for the variation of properties. The ratio of viscosity was estimated by computing wall temperatures from the accepted Colburn equation for pipe flow. It is important to note that the high temperature runs are in agreement with the cold pressure-drop runs even though the results are based upon readings 1½ ft apart and the properties vary along the test section.

Two-phase flow

Two-phase pressure-drop runs were performed for all the geometries studied in single-phase flow. A typical set of measurements is reproduced in Fig. 9. The effects of eccentricity upon two-phase pressure drop cannot be as clearly defined as for single-phase flow. The major reason is that the flow system is vertical and calculations of two-phase frictional losses require postulating the steam slip in terms of quality. While the steam void data given in [8] at 1000 lbf/in² could be utilized, it is not apparent how these data could be applied to eccentric rod geometries without making an assumption about flow channeling. A preliminary estimate of eccentricity effects, however, can be obtained from Fig. 10. Here two sets of two runs as nearly similar as possible are plotted. By examination of the pressure losses in terms of steam quality it is noted that in both instances the pressure drop is slightly lower as the eccentricity is raised. The difference in pressure drop is, however, very small. A more detailed discussion of this point is given in a later section.

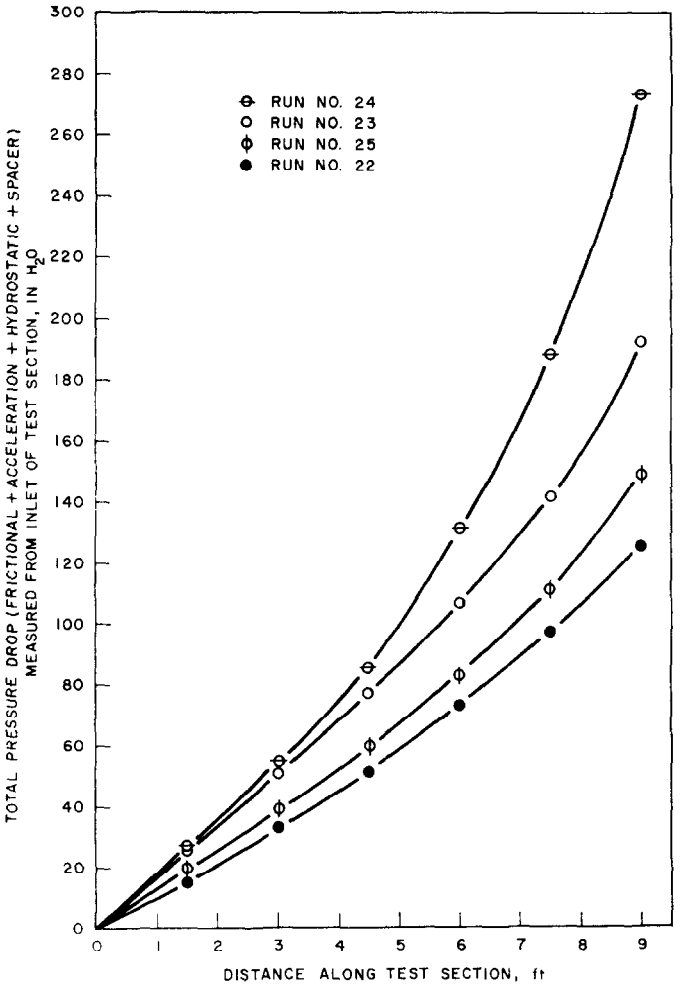

FIG. 9. Two-phase pressure drop for concentric rod.

An analytical model is postulated there which relies upon the data of [8]. The model which subdivides the flow region into two zones is used to evaluate the accuracy of the steam slip data of [8] and the pressure-drop relations of Martinelli–Nelson [9].

TEST RESULTS—BURNOUT

Effect of eccentricity

To investigate the effects of eccentricity, burnout tests were performed at 1000 lbf/in^2 with a concentric rod and with three displaced rod geometries. The minimum flow annulus was successively reduced to 0·096, 0·061 and 0·033 in compared to a concentric flow spacing of 0·1675 in. All test results are tabulated in Table 3.

Burnout values for a concentric rod are shown in Fig. 11. Co-ordinates of burnout heat flux versus steam quality, used therein, are those proposed in [4]. It is noticed that the spread in experimental results is ± 10 per cent or just about within the maximum error range of the system. The test results also fall above the recommended design line of [3].

Test results for a 0·096 in minimum flow

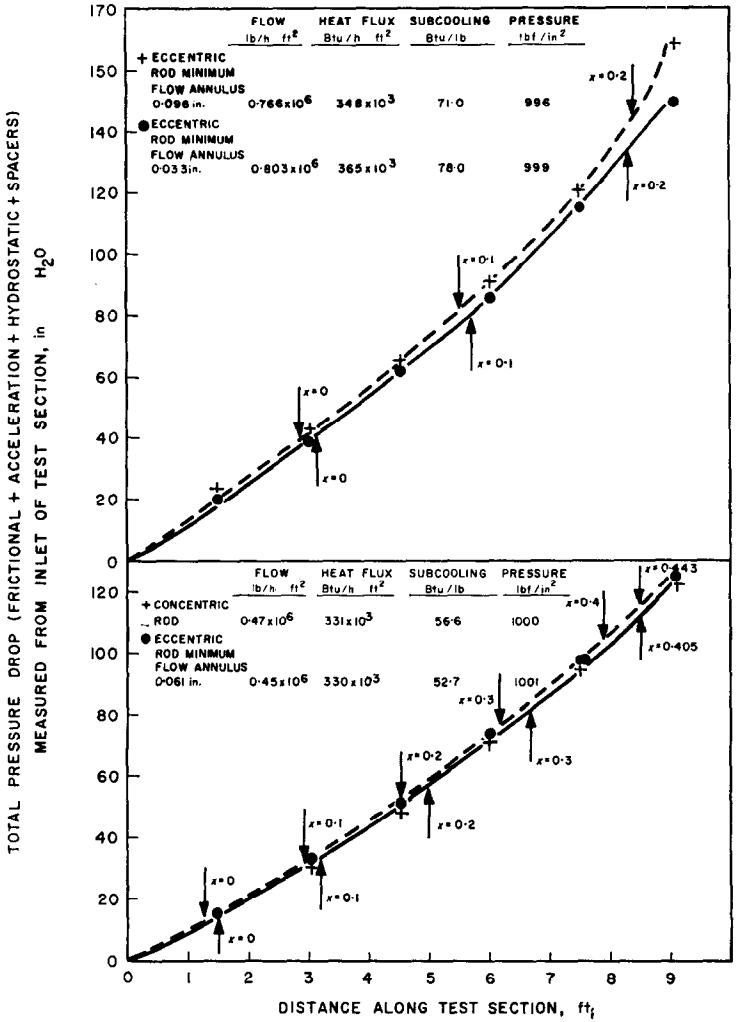

FIG. 10. Effect of eccentricity upon two-phase pressure drop.

annulus are plotted in Fig. 12. The mean straight line drawn through the concentric data is reproduced here for comparison purposes. It is seen that excellent agreement is obtained between this eccentric geometry and the concentric rod case. For all practical purposes, no reduction in burnout heat flux was obtained by displacement of the rod about 50 per cent of the flow channel distance. Note again that the experimental-data spread is small and below 10 per cent. The repeatability of test results is also illustrated by the close grouping of four points at a steam quality of 32 per cent.

Burnout fluxes for a minimum flow annulus of 0·061 in are also shown in Fig. 12. Data for the 0·061 in minimum flow annulus agree with the previous results. Test runs are once again correlated within $\pm$ 10 per cent.

The results for a minimum flow annulus of 0·033 in are plotted in Fig. 13. A greater departure from previous runs is noted and the deviation decreases as the steam quality increases. A mean curve through the experimental data can be drawn to obtain a correlation within $\pm$ 15 per cent. Closer examination of the figure, however, reveals that, for this geometry,

Table 3. Burnout data

Run	Minimum flow annulus (in)	Flow ($\times 10^{-6}$) (lb/h ft^2)	Subcooling (Btu/lb)	Pressure (lbf/in^2)	Heat flux ($\times 10^{-3}$) (Btu/h ft^2)	Exit quality (wt.—%)
38	0·1675	0·261	70·7	1003	263	61·5
39	0·1675	0·337	60·1	1002	296	53·6
40	0·1675	0·559	63·8	1006	375	38·1
41	0·1675	0·909	60·9	1004	454	27·6
42	0·1675	0·997	165·0	1007	647	21·0
43	0·1675	1·14	266·6	997	892	14·8
44	0·1675	1·19	54·9	1002	513	22·3
45	0·1675	0·955	82·3	1001	513	25·9
46	0·1675	0·742	172·0	1012	514	23·1
47	0·1675	1·17	72·9	999	528	20·8
48	0·1675	1·16	71·9	1002	524	21·3
49	0·096	0·772	58·8	955	448	32·1
50	0·096	1·07	126·0	1000	606	21·1
51	0·096	1·19	238·0	993	840	13·6
52	0·096	1·19	252·0	967	889	14·5
53	0·096	0·764	60·0	998	439	31·8
54	0·096	0·351	47·3	950	315	56·2
55	0·096	0·747	60·6	1002	429	31·8
56	0·096	0·422	83·8	1003	359	48·1
57	0·096	0·999	74·1	1023	505	24·8
58	0·096	1·17	184·0	1012	752	16·2
59	0·096	0·767	63·8	1006	436	30·4
60	0·061	0·815	96·2	1001	479	27·3
61	0·061	0·442	51·9	990	332	45·9
62	0·061	1·29	263·0	975	938	11·5
63	0·061	0·922	216·0	1027	663	18·6
64	0·061	1·32	264·0	825	967	11·1
65	0·061	1·34	294·0	755	1040	9·3
66	0·061	0·819	101·0	1000	471	25·6
67	0·033	0·811	101·0	1002	443	23·5
68	0·033	0·553	51·3	1010	354	38·1
69	0·033	0·248	186·0	1014	275	65·5
70	0·033	1·23	284·0	1001	616	8·5
71	0·033	0·809	208·0	1001	446	24·2
72	0·033	0·98	296·0	780	771	10·0
73	0·033	0·98	299·0	795	771	10·1
74	0·033	1·15	25·3	1005	427	22·6
75	0·033	1·14	107·0	1022	539	17·7
76	0·033	0·835	194·0	985	580	19·8
77	0·033	0·14	151·0	1001	625	16·1
78	0·033	0·81	30·1	1004	397	30·7
79	0·033	0·535	39·2	1000	348	40·5

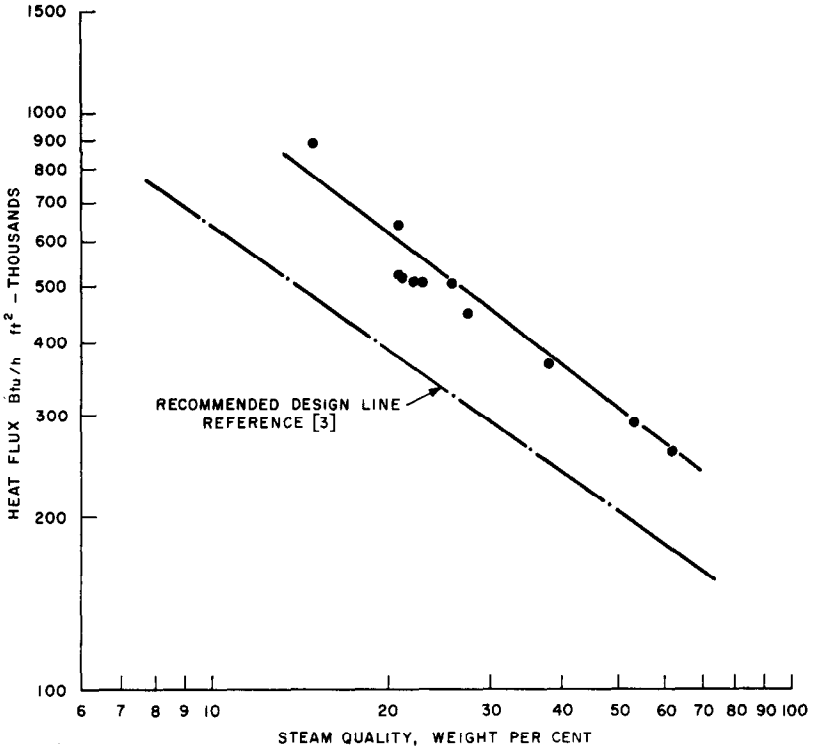

FIG. 11. Burnout data for concentric annulus at 1000 lbf/in².

a flow effect can be detected. The mass flow rate for each run is shown in brackets in Fig. 13. One notes that the burnout heat flux decreases as the flow rate increases.

In order to ascertain that the burnout heat flux decrease was due to rod eccentricity rather than increased flow, burnout data obtained at flow rates of 0·9–1·3 $\times$ 10^6 lb/h ft² were plotted in Fig. 14. It is seen that the test data obtained with the concentric rod and 0·096 and 0·061 minimum annuli agree, while a definite reduction of about 15–30 per cent is obtained for the 0·033 in minimum annulus.

The over-all reduction in Fig. 14 in burnout heat flux is still relatively small when it is realized that the flow annulus on one side of the rod is only one-fifth what it used to be. One can, therefore, surmise that some mixing is taking place in the two-phase mixture. Still, burnout occurs on the eccentric side. Thermocouple readings verified it, and examination of the test section revealed a localized burnout area on the eccentric side.

A comparison of the present test data with available test results at 1000 lbf/in² at high L/D ratios is given in Fig. 15. Agreement is noted with some of the UCLA data at low steam quality and some of the Bettis data at high steam quality. Further comparison between the three sets of information is not warranted until a better understanding of burnout is obtained. Several explanations can be advanced for the experimental deviations in Fig. 15.

(1) It is possible that experimental techniques need improvement. Main sources of error in the authors' opinion are false burnouts, variation in test-section geometry during operation, and experimental inaccuracies.

(2) Another possibility is that one of the controlling variables was not included in the correlations. Recent investigations have shown that flow rate plays an important role [10]. It

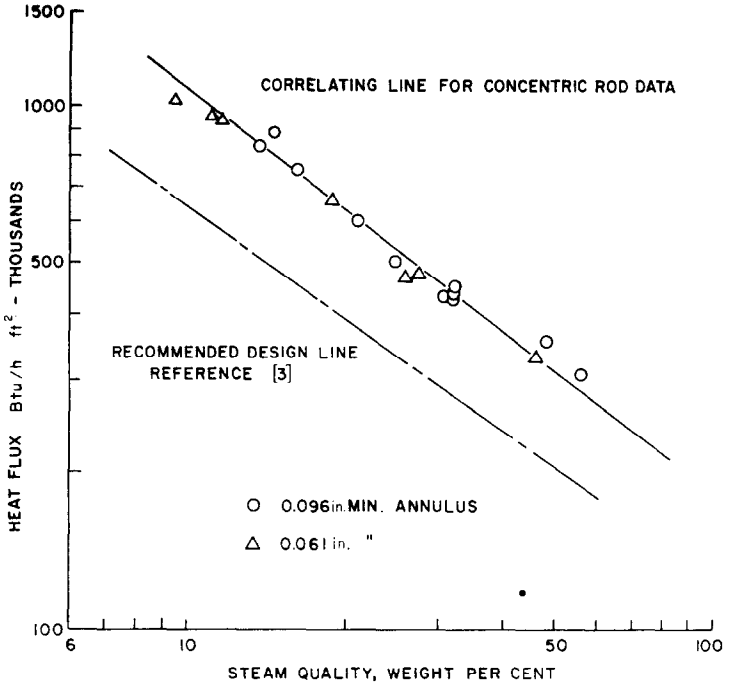

FIG. 12. Burnout data at 1000 lbf/in² for eccentric rod with 0·096 in and 0·061 in minimum flow annulus.

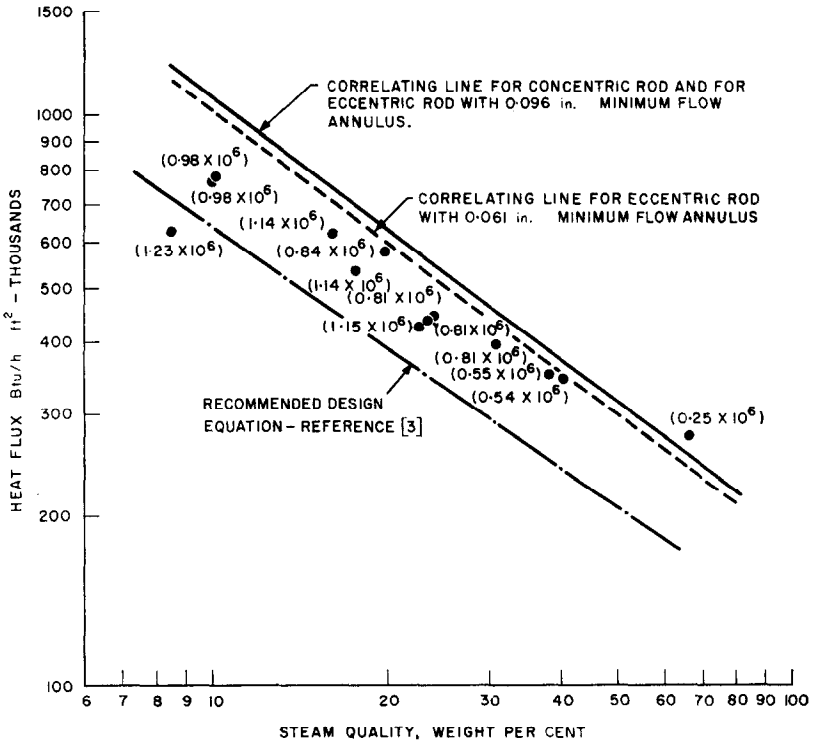

FIG. 13. Burnout data for eccentric rod with 0·033 in minimum flow annulus.

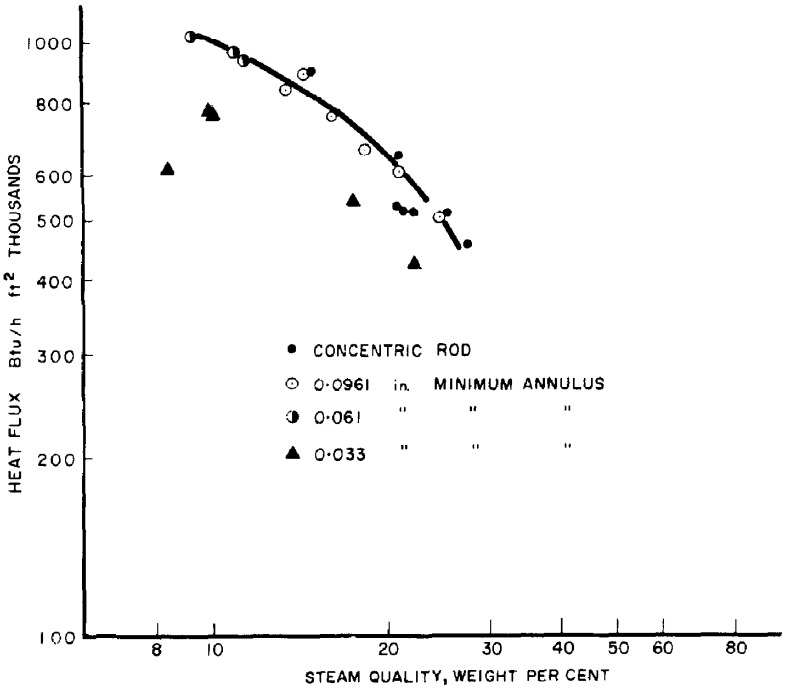

FIG. 14. Effect of rod eccentricity upon burnout data for constant flow rate range of $0{\cdot}9–1{\cdot}3 \times 10^6$ lb/h ft².

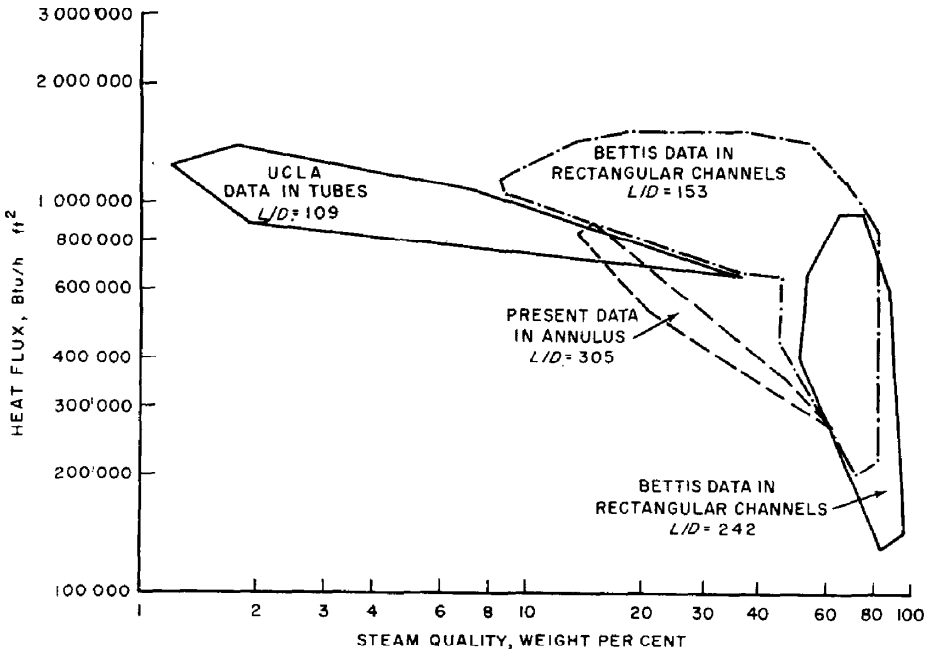

FIG. 15. Comparison of present results with available burnout data.

must also depend upon the flow characteristics at the exit end of the rod. Different burnout values for short and long heated rods tend to verify this. Two-phase pressure-drop flow pattern, and steam slip may be expected to vary with heated length, heat flux and flow. Correlations to date may be inadequate because they cannot account for these variables.

(3) Another area of uncertainty is the role played by the test loop. Deviations arising from different investigations indicate that the loop system must affect the results. In [11] the effects of loop geometry were underscored. A very stable circuit with very high head pump could lead to higher burnout heat fluxes than a low head loop.

ANALYSIS—ECCENTRIC ROD

Method of solution

An analysis was undertaken to determine the degree of mixing in an eccentric rod geometry. The basic model used in the analysis subdivides the flow area into two parallel channels, as shown in Fig. 16. The pressure drop in the flow direction is assumed the same for the two channels and the flow rate and steam quality in each channel is accordingly adjusted. The distribution of steam quality within the fuel assembly is then obtained step-by-step in the flow direction. The equations are derived in [12]. They can be solved once the channel geometry and heat-transfer characteristics are specified.

The calculations are based upon the following assumptions:

(1) Two-phase pressure drop was obtained from the correlation of Martinelli and Nelson [9].
(2) Experimental void data of Larson [8] at 1000 lbf/in^2 were utilized in the computations. Corrections have been made to allow for voids in the subcooled region in terms of fuel-rod heat flux.
(3) The friction factor was assumed to be the same for the two flow channels and to remain constant in the flow direction.
(4) The change in mass flow rate in each channel was neglected compared to the change in quality over the small incremental length used in the calculations.
(5) The pressure loss due to spacers was apportioned over a finite interval which can be specified.

Results

Several cases were computed on an IBM-650. A typical set of results is shown in Fig. 16 for a minimum flow annulus of 0·090 in.* By varying the size of the two parallel flow channels the degree of mixing can be estimated by comparison with the experimental data. The analytical model in Fig. 16 indicates that the mixing extends well over half of the flow area, if the steam quality in the eccentric zone is not to produce burnout. Also, it appears that transverse mixing extends over the entire cross section and that only the transverse flow time lag accounts for the reduction in burnout. This is all the more apparent when the model is utilized at higher eccentricites. For instance, for a minimum flow annulus of 0·061 in, the maldistribution of flow is about 30 per cent larger and the results point to a greater and greater mixing zone.

Pressure drop curves corresponding to Fig. 16 are shown in Fig. 17. Examination of the predicted two-phase pressure drops shows that they are not highly dependent upon the assumed flow geometry. The analytical model can, therefore, be effectively used to evaluate the relations of Martinelli–Nelson and Larson by comparison with the experimental pressure-drop results. Test and calculated values are given in Table 4 and the discrepancy between measurements and predictions falls below 10 per cent.† The analytical model thus approximately confirms the validity of the Martinelli–Nelson and Larson relations.

ACKNOWLEDGEMENT

The authors wish to acknowledge the assistance of J. A. Kervinen and F. S. Raczynski in loop operation.

* For simplification purposes, spacers were left out from this preliminary analysis. Later calculations indicated that their presence accentuated the flow maldistribution.

† The analysis does not allow for variation of the friction factor with subcooling and is based upon a friction factor calculated for saturated conditions.

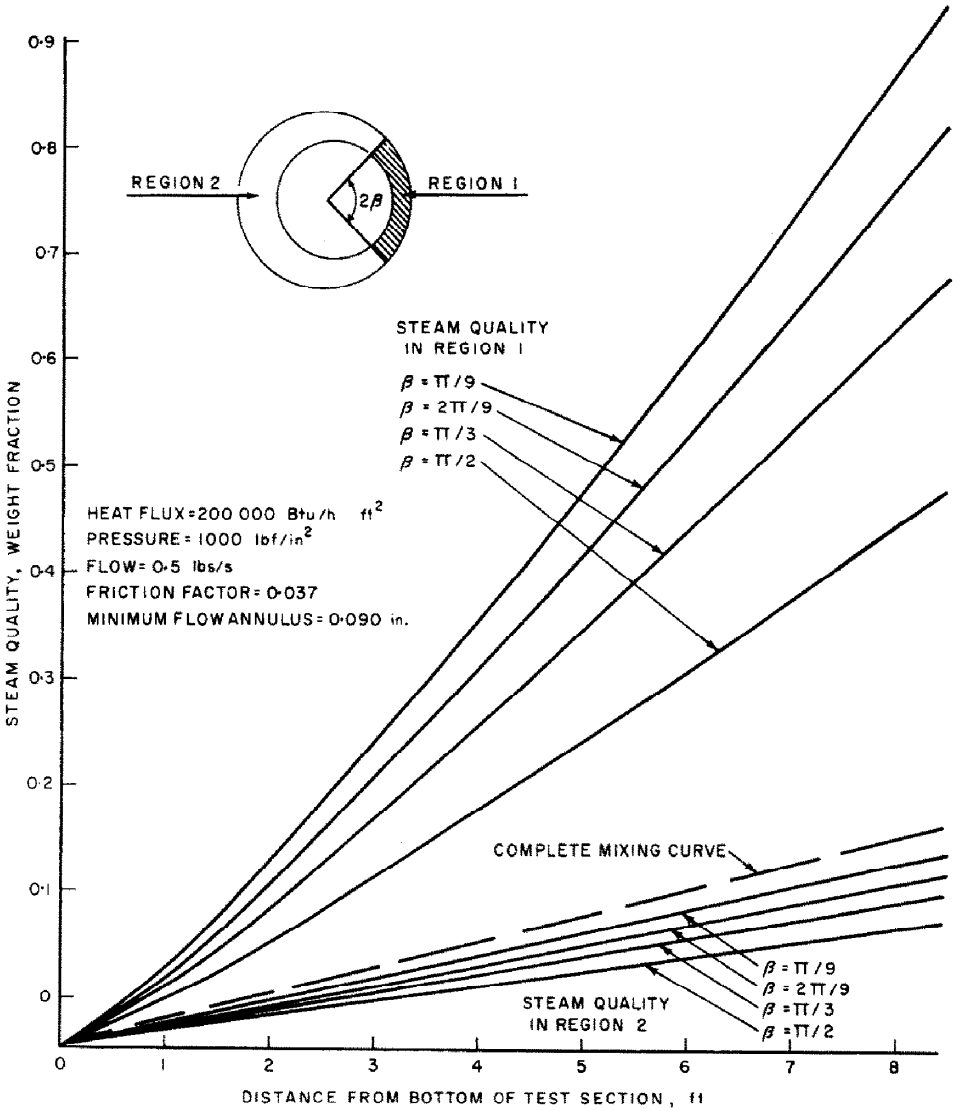

FIG. 16. Eccentric-rod analysis—steam distribution in terms of assumed mixing.

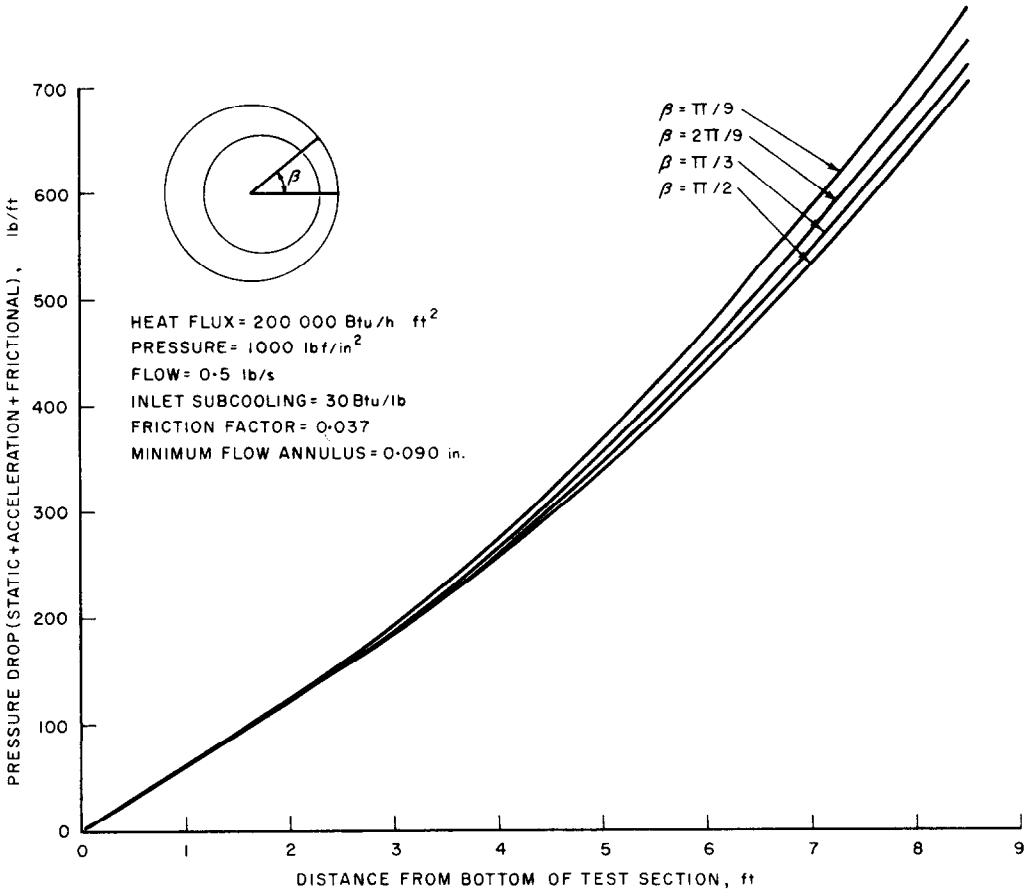

FIG. 17. Eccentric-rod analysis—two-phase pressure-drop prediction in terms of assumed mixing.

Table 4. Comparison of measured and predicted two-phase pressure drop based upon measured single-phase friction factor

Position along test section, (ft)	Pressure drop (in H_2O) Run no. 23		Run no. 24		Run no. 25	
	Measured	Calculated	Measured	Calculated	Measured	Calculated
0–1·5	26·2	23·7	26·3	24·1	19·9	17·5
0–3	51·1	47·7	53·5	49	39·1	34·9
0–4·5	77	70·9	85·5	76·3	59	51·2
0–6	106·7	95·2	131·5	130	82·8	72·8
0–7·5	141·5	128·5	188	202	111	104·8
0–8·5		173		255		129·7
0–9	192		273		148·5	

REFERENCES

1. R. P. STEIN, J. W. HOOPES, JR., M. MARKELS, JR., W. A. SELKE, A. J. BENDLER and C. F. BONILLA, Pressure drop and heat transfer to non-boiling and boiling water in turbulent flow in an internally heated annulus. *Chem. Engng Progr. Symp. Ser.* **50** No. 11, 115–126 (1954).
2. L. H. MCEWEN, D. J. FOLEY and M. R. KREITER, Heat transfer beyond burnout. *Amer. Soc. Mech. Engrs*, Paper No. 57-SA-49 (1957).
3. A. E. GALSON and E. E. POLOMIK, Burnout data applicable to boiling water reactors, *ANS Pittsburgh Meeting*, June (1957).
4. R. A. DEBORTOLI, S. J. GREEN, B. W. LETOURNEAU, M. TROY and A. WEISS, Forced convection heat transfer burnout studies for water in rectangular channels and round tubes at pressures above 500 lb/in². *WAPD*-188, October (1958).
5. S. LEVY, E. E. POLOMIK, C. L. SWAN and A. W. MCKINNEY, Eccentric rod burnout at 1000 lb/in² with net steam generation. *General Electric Report* 3148 (1959).
6. S. J. KLINE and F. A. MCCLINTOCK, Describing uncertainties in single sample experiments. *Mech. Engng, N.Y.* **75**, No. 1, 3–8 (1953).
7. Quart. Progr. Rep. IX-QPR-1-61, Columbia University, 1 Jan. to 31 Mar. (1961).
8. H. C. LARSON, Void fractions of two-phase steam–water mixture. Thesis, University of Minnesota (1957).
9. R. C. MARTINELLI and D. B. NELSON, Prediction of pressure drop during forced circulation boiling of water. *Trans. Amer. Soc. Mech. Engrs.* **70**, No. 6, 695–702 (1948).
10. A. CICCHITTI, M. SILVESTRI, G. SOLDAINI and R. ZARATELLI, A critical survey of the literature on burnout studies with wet steam. *Energia Nucleare*, **6**, No. 10, 637–660 (1959).
11. W. H. LOWDERMILK, C. D. LANZO and B. L. SIEGEL, Investigation of boiling burnout and flow stability for water flowing in tubes. *NACA* TM 4382 (1958).
12. S. LEVY and A. W. MCKINNEY, Calculation of steam distribution in a multi-rod assembly on an IBM-650 (Code PARCH). *General Electric Report* 3125, March (1959).

Résumé—Des essais de perte de charge et de combustion totale ont été faits avec des barres décentrées pour simuler une mauvaise distribution de l'écoulement dans des réacteurs multi-barres à eau bouillante. Des valeurs numériques sont données pour une barre (13,5 mm de diamètre et 250 cm de long) chauffée uniformément et placée dans une conduite circulaire de 22 mm de diamètre. Les expériences ont été faites pour quatre positions de la barre (une disposition concentrique et trois dispositions décentrées) des densités de vapeur à la sortie variant de 9 à 66%, des débits de $1{,}25.10^{-4}$ à $6{,}6.10^{2}$ kg/cm² h et des pressions de 70 kg/cm². Les résultats sont les suivants:

1° Les flux thermiques pour une combustion totale avec une production de vapeur "net" sont les mêmes pour un espace d'écoulement concentrique de 4,25 mm et un espace décentré de 2,46 à 1,55 mm. Les valeurs décroissent de 15 à 36% quand l'espace d'écoulement minimum est réduit de de 4,25 mm à 0,85 mm.

2° Les essais de perte de charge en présence d'une seule phase montre une diminution du facteur de frottement quand l'excentricité croît. D'autre part, les pertes de charge en présence de deux phases restent relativement les mêmes pour les différentes excentricités.

3° L'auteur propose un modèle d'étude pour la détermination du degré de mélange transversal dans la disposition excentrée. Ce modèle, basé sur la subdivision de la section d'écoulement en deux conduites parallèles indique que le mélange s'étend au moins sur la moitié de la zone d'écoulement.

Zusammenfassung—Burnout- und Druckverlustuntersuchungen wurden an einer exzentrischen Stabanordnung durchgeführt, um eine mögliche Fehlverteilung des Kühlstroms im Brennstabbündel eines Siedewasser-Reaktors nachzuahmen. Die ermittelten Daten erstreckten sich auf einen 2,6 m langen, gleichmässig beheizten Stab vom Durchmesser 1,37 cm, der in einem zylindrischen Rohr von 2,22 cm Innendruchmesser angeordnet war. Die Versuchsvariation umfasste eine konzentrische und drei exzentrische Stabanordnungen, einen Austrittsdampfgehalt von 9 bis 66 Gewichtsprozent und Durchsatzmengen von 325 bis 1724 kg/m²s bei Drücken im System von ca 70 bar. Die Ergebnisse waren:

(1) Die Wärmestromdichten für Burnout bei Reindampferzeugung sind für den konzentrischen Ringraum von 0,4254 cm Breite und bei Exzentrizität für eine minimale Spaltbreite von 0,244 und 0,155 cm die gleichen. Bei Verkleinerung der Minimalspaltbreite von 0,4254 auf 0,084 cm nehmen die Burnout-Werte um 15 bis 36% ab.

(2) Die Druckverluste bei Einphasenströmung zeigen eine Abnahme der Reibungszahl bei zunehmender Exzentrizität. Dagegen bleiben die Druckverluste bei Zweiphasenströmung für verschiedene Exzentrizitäten relativ unverändert.

(3) Um den Grad der Quervermischung bei exzentrischer Anordnung zu bestimmen, wurde ein analytisches Modell angenommen. Dieses Modell beruht auf einer Unterteilung des Strömungsquerschnitts in zwei parallele Kanäle. Es führt zu dem Schluss, dass sich die Vermischung gut über die halbe Strömungszone erstreckt.

Аннотация—Опыты по выгоранию и перепаду давлений проводились со стержнем эксцентрического сечения для того, чтобы имитировать возможную неравномерность распределения потока во многостержневых топливных устройствах кипящих реакторов. Приведены данные для равномерно нагретого стержня диаметром 0,540 дюйма и длиной 8½ фута, помещенного в круглую трубу с внутренним диаметром 0,875 дюйма. Опыты проводились при следующих изменениях условий: концентрическое расположение стержня и смещенное (три); весовое паросодержание на выходе от 9 до 66%; скорость потока от 0,25 до 1,34 × 10^6 фунтов в час на кв.фут при давлении в системе в 1000 фунтов на кв.дюйм. Результаты опытов следующие:

(1) Потоки тепла от сгорания при полной генерации тепла одинаковы для концентрического кольцевого канала 0,1675 дюйма и эксцентрического с минимальной шириной 0,096 и 0,061 дюйма. Величина выгорания уменьшается на 15–36%, если минимальную ширину эксцентрического кольцевого канала уменьшить с 0,1675 до 0,033 дюйма.

(2) Опыты по определению перепада давления однофазной жидкости показывают снижение коэффициента трения при увеличении эксцентриситета. С другой стороны, потери давления в двухфазном потоке остаются примерно такими же при различных значениях эксцентриситета.

(3) Предложена аналитическая модель для определения степени поперечного перемешивания в эксцентрических кольцевых каналах. Модель, основанная на разделении сечения потока на два параллельных канала, показывает, что смешение хорошо распространяется на половину зоны течения.